# Spatial positioning of CFTR's pore-lining residues affirms an asymmetrical contribution of transmembrane segments to the anion permeation pathway

Xiaolong Gao[1,2] and Tzyh-Chang Hwang[1,2,3]

[1]Dalton Cardiovascular Research Center, [2]Department of Biological Engineering, and [3]Department of Medical Pharmacology and Physiology, University of Missouri, Columbia, MO 65211

The structural composition of CFTR's anion permeation pathway has been proposed to consist of a short narrow region, flanked by two wide inner and outer vestibules, based on systematic cysteine scanning studies using thiol-reactive probes of various sizes. Although these studies identified several of the transmembrane segments (TMs) as pore lining, the exact spatial relationship between pore-lining elements remains under debate. Here, we introduce cysteine pairs in several key pore-lining positions in TM1, 6, and 12 and use $Cd^{2+}$ as a probe to gauge the spatial relationship of these residues within the pore. We find that inhibition of single cysteine CFTR mutants, such as 102C in TM1 or 341C in TM6, by intracellular $Cd^{2+}$ is readily reversible upon removal of the metal ion. However, the inhibitory effect of $Cd^{2+}$ on the double mutant 102C/341C requires the chelating agent dithiothreitol (DTT) for rapid reversal, indicating that 102C and 341C are close enough to the internal edge of the narrow region to coordinate one $Cd^{2+}$ ion between them. We observe similar effects of extracellular $Cd^{2+}$ on TM1/TM6 cysteine pairs 106C/337C, 107C/337C, and 107C/338C, corroborating the idea that these paired residues are physically close to each other at the external edge of the narrow region. Although these data paint a picture of relatively symmetrical contributions to CFTR's pore by TM1 and TM6, introducing cysteine pairs between TM6 and TM12 (348C/1141C, 348C/1144C, and 348C/1145C) or between TM1 and TM12 (95C/1141C) yields results that contest the long-held principle of twofold pseudo-symmetry in the assembly of ABC transporters' TMs. Collectively, these findings not only advance our current understanding of the architecture of CFTR's pore, but could serve as a guide for refining computational models of CFTR by imposing physical constraints among pore-lining residues.

The Journal of General Physiology

## INTRODUCTION

Regulated ion movement across the cell membrane by transport proteins partakes in a broad array of physiological functions in the human body; hence, it is not surprising that disruptions of this process could lead to many disease states (Cooper and Jan, 1999). Among them, cystic fibrosis (CF) ails the suffered from their birth because of a defective chloride transport across the epithelial cells in the airway, the gastrointestinal tract, and the reproductive system (Riordan et al., 1989). Although CFTR—the culprit behind CF—is a bona fide anion channel, topological analysis of its amino acid sequence (Dean and Annilo, 2005) places CFTR in the superfamily of the ABC transporter (Riordan et al., 1989). Like most exporter members of this superfamily, CFTR possesses the prototypical architecture of two transmembrane domains (TMDs; TMD1 and TMD2), each followed by a cytoplasmic nucleotide-binding domain (NBD; NBD1 and NBD2). Each TMD consists of 6 transmembrane segments (TMs), and some of the overall 12 TMs have been shown to craft an anion-selective pore (Akabas et al., 1994; Alexander et al., 2009; Bai et al., 2010, 2011; El Hiani and Linsdell, 2010; Qian et al., 2011; Wang et al., 2011, 2014; Norimatsu et al., 2012; Gao et al., 2013; Zhang and Hwang, 2015). In contrast, the two NBDs play a key role in controlling opening/closing of the gate in TMDs. Specifically, after ATP binding to the two binding pockets formed by NBDs, dimerization of the two NBDs facilitates gate opening, whereas gate closure is greatly accelerated by ATP hydrolysis-induced disruption of the NBD dimer (Csanády and Gadsby, 1999; Gadsby and Nairn, 1999b; Jih and Hwang, 2012). In addition to these characteristic domains shared by other ABC proteins, CFTR distinguishes itself from its peers in this superfamily by harboring a unique intracellular regulatory domain (R domain) where several conserved serine/threonine residues must be phosphorylated in order for ATP to gate the channel (Gadsby and Nairn, 1999a).

Along with the aforementioned topological similarities between CFTR and ABC exporters, functional resemblance that NBD dimerization triggers the gates in the TMDs to open has led to the proposition that CFTR

Correspondence to Tzyh-Chang Hwang: hwangt@health.missouri.edu

Abbreviations used in this paper: αHL, α-hemolysin; DTT, dithiothreitol; NBD, nucleotide-binding domain; SCAM, substituted cysteine accessibility method; TM, transmembrane segment; TMD, transmembrane domain.



The Rockefeller University Press $30.00
J. Gen. Physiol. 2016 Vol. 147 No. 5 407–422
www.jgp.org/cgi/doi/10.1085/jgp.201511557

may evolve from a primordial ABC exporter by degrading its cytoplasmic gate (Gadsby et al., 2006; Chen and Hwang, 2008). So far, high-resolution structures of eight ABC exporters have been solved (Dawson and Locher, 2006; Ward et al., 2007; Aller et al., 2009; Hohl et al., 2012; Jin et al., 2012; Shintre et al., 2013; Choudhury et al., 2014; Kodan et al., 2014). Regardless of whether the whole protein is composed of two identical halves or not, a twofold (pseudo) symmetry of the substrate translocation pathway is found. Experiments on CFTR's pore-lining TM6 and TM12 also appear to support such a symmetrical contribution of TM6 in TMD1 and its counterpart TM12 in TMD2 to the internal vestibule of the pore by demonstrating that cysteines introduced into the cytoplasmic portion of these two pore-lining TMs could be accessed by intracellular MTS reagents in both the open and the closed states (Bai et al., 2011). However, recent studies provided more details in the structural and functional roles of CFTR's TMDs. For example, although several studies assure a pore-lining role for TM1 in CFTR (Akabas et al., 1994; Wang et al., 2011; Gao et al., 2013), overwhelming evidence argues against such a role for TM7 (Wang et al., 2014; Zhang and Hwang, 2015), the counterpart of TM1, in pore construction, countering the long-held twofold pseudo-symmetry in the TMDs of ABC exporters. Furthermore, the extracellular end of ABC exporters' substrate translocation pathway closes to form a gate for the substrates (Kodan et al., 2014), but the external entryway of CFTR's pore is accessible to extracellular anions in a closed channel (Gao and Hwang, 2015). Specifically, our latest studies suggest that CFTR's gate (between positions 337 and 344 in TM6) coincides with the previously identified narrow region of the pore that spans a short segment in TM6 (positions 338 to 341; Alexander et al., 2009; Bai et al., 2010). Interestingly, our cysteine scanning experiments on TM1 also identified a narrow region confined in between L102 to I106, which prevents bulky MTS reagents from passing through the channel (Gao et al., 2013). Therefore, the narrowest section in CFTR's pore could be as short as just one α-helical turn in length if both TM1 and TM6 indeed, as proposed, assume a secondary structure of an α-helix (Alexander et al., 2009; Bai et al., 2010; El Hiani and Linsdell, 2010; Gao et al., 2013). In addition to this narrow segment, the pore of CFTR comprises two flanking compartments known as internal and external vestibules (Liu et al., 2003; Linsdell, 2014; Gao and Hwang, 2015), which are relatively wide based on the observations that many bulky reagents, like MTS reagents or channel blockers (e.g., glibenclamide), can be accommodated in these regions (Sheppard and Robinson, 1997; Zhou et al., 2002; Bai et al., 2010, 2011; Gao et al., 2013).

As described above, our molecular understanding of CFTR's pore and gate has been fostered immensely by a plethora of functional studies, but the relative positions of the pore-lining residues as well as the alignment between individual TMs remain unclear, lacking a high-resolution structure of CFTR's TMDs. Some recent experiments using the cross-linking strategy by engineering cysteine pairs do provide some insights into the positional relationship between pore-lining residues in the spacious internal vestibule (El Hiani and Linsdell, 2014). However, when mapped to homology models of CFTR (e.g., those in Corradi et al. [2015]), those supposedly cross-linkable residues are located too far away from each other than expected from the cross-linking data shown in El Hiani and Linsdell (2014). (See Fig. 1 legend for more details.) What is also surprising is a lack of studies tackling the regions close to the narrow region, which could be ideal for cross-linking experiments because of its physical constraints. Of note, although our previous study has proposed a revised topology for TM1 that places L102 residue at the internal edge of the narrow region, and hence close to S341 the corresponding position in TM6 (Gao et al., 2013), a quite different picture was depicted by another study (Wang et al., 2011). To fill these knowledge gaps, we used the paired cysteine strategy and performed more extensive experiments on TMs 1, 6, and 12, the three most extensively investigated pore-lining TMs, with a special emphasis on the residues just internal or external to the narrowest segment of the pore.

We introduced cysteine pairs to several positions in those three TMs and used $Cd^{2+}$ as our probe to test the formation of any "tight" $Cd^{2+}$-binding sites by the introduced paired thiol groups. We found that although $Cd^{2+}$-induced inhibition on all mutants carrying one single cysteine (except for 344C) could be reversed rapidly upon simple removal of $Cd^{2+}$ from the perfusate, this inhibitory effect on mutants with cysteine pairs 102C/341C, 106C/337C, 107C/337C, and 107C/338C becomes nearly irreversible. The observation that dithiothreitol (DTT), a strong $Cd^{2+}$ chelator (Krężel et al., 2001) that may have better access to $Cd^{2+}$-thiol metal bridges than EGTA because of its smaller size, can rapidly reverse the effects brought by $Cd^{2+}$ implicates the formation of a metal bridge between these paired cysteines. These results are consistent with our previous cysteine scanning studies (Bai et al., 2010; Gao et al., 2013) and hence support the notion that TM1 and TM6 contribute to all three components of the pore. When we used the same approach to examine the relation between TM6 in TMD1 and its topological counterpart in TMD2, TM12, surprisingly, our data suggested that the previously defined middle section of TM12 (e.g., position 1141) does not align with the topologically equivalent position in TM6 (i.e., S341). Instead, 1141C forms a tight $Cd^{2+}$-binding site with the engineered cysteine at position 348 in TM6, which is two helical turns internal to the S341 residue. A similar $Cd^{2+}$-binding site was im-

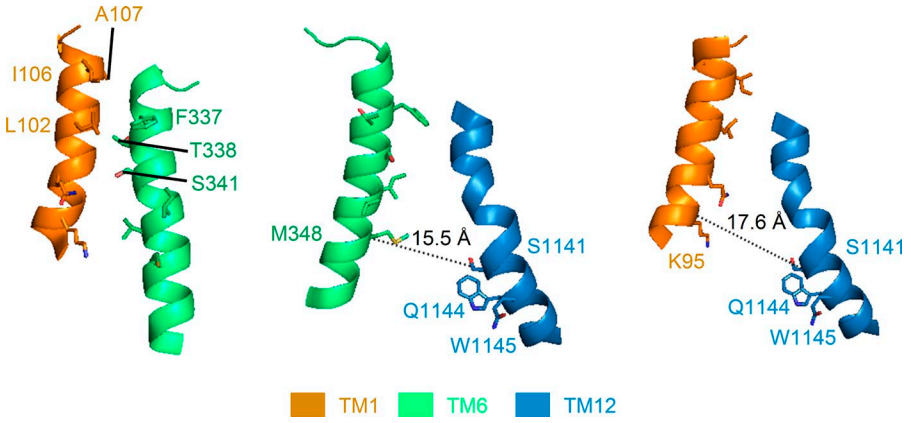


Figure 1. **Relative alignments among TM1, TM6, and TM12 depicted in a CFTR homology model.** Based on the crystal structure of an asymmetrical ABC transporter, TM287/288, Corradi et al. (2015) derived a CFTR model in which the alignment between TM1 and TM6 (left) is fairly consistent with data represented in the current work. However, the distance between several positions where introduced cysteines were shown to be cross-linkable (El Hiani and Linsdell, 2014) is way beyond the physical constrain for the formation of an effective $Cd^{2+}$ metal bridge. For example, the distance between M348 and S1141 (15.5 Å, middle) and that between K95 and S1141 (17.6 Å, right) both well exceed the working distance of $Cd^{2+}$, the cross-linker used in El Hiani and Linsdell (2014). Note that although the distances measured above are between α-carbons of the two residues involved, the minimum sulfur to sulfur distance between two engineered cysteines, calculated by subtracting 5.6 Å (twice the distance of a single cysteine side chain) from the above values (i.e., 9.9 Å for 348C and 1141C; 12 Å for 95C and 1141C), is still >6.5 Å, the distance for coordination of two thiol groups with $Cd^{2+}$.

plicated between 1141C and 95C, the latter of which again is two helical turns cytoplasmic to the inner edge of the narrow region in TM1 (i.e., position 102). Collectively, the current study not only assigns specific amino acid residues that confine the functionally important region of the pore, but also provides experimental evidence echoing the idea of an asymmetrical construction of CFTR's pore by its two TMDs.

## MATERIALS AND METHODS

### Mutagenesis and channel expression

The cysless background construct used in the current study was first made where 16 out of the overall 18 endogenous cysteines in CFTR were mutated to serines with the rest of 590C and 592C mutated to leucines (Mense et al., 2006). As described in Wang et al. (2007), an additional V510A mutation was introduced to all constructs to boost channel expression. Subsequently, site-directed mutagenesis was performed under this cysless background to engineer cysteines at positions of interest. All mutations were confirmed by DNA sequencing (DNA core, University of Missouri).

Chinese hamster ovary (CHO) cells grown in Dulbecco's modified Eagle's medium with 10% fetal bovine serum were used to express CFTR channels. Together with pEGFP-C3, which encodes the green fluorescence protein, all constructs were transfected into CHO cells using PolyFect reagent (QIAGEN), according to the instructions from the manufacturer. Electrophysiological data were collected 3–7 d after transfection.

### Electrophysiology

**Inside-out mode.** Pipettes were made by pulling the borosilicate capillary glass using a vertical puller (Narishige). After fire polishing with a homemade microforge, the resistance of pipettes was between 1.5 MΩ and 2.5 MΩ when filled with the inside-out pipette solution, which contained (mM) 140 NMDG-Cl, 2 $MgCl_2$, 5 $CaCl_2$, and 10 HEPES, with pH adjusted to 7.4 using NMDG. Before every experiment, cells expressing certain mutants were transferred into a chamber that was initially filled with a bath solution containing (mM) 145 NaCl, 5 KCl, 2 $MgCl_2$, 1 $CaCl_2$, 5 glucose, 5 HEPES, and 20 sucrose, with pH adjusted to 7.4 using NaOH. After a tight GΩ seal was made, yet before our excising the patch into the inside-out mode, the background flow was switched to the standard inside-out perfusate containing (mM) 150 NMDG-Cl, 8 Tris, 10 EGTA, 2 $MgCl_2$, and 10 HEPES, with pH adjusted to 7.4 using NMDG. All inside-out perfusion solutions contained EGTA except for the one containing $Cd^{2+}$. In addition, to ensure most of the cysteines in the patch were in their reduced form, DTT was added into the PKA/ATP cocktail used routinely to activate the channels. All experiments with $Cd^{2+}$ were performed after CFTR currents had been activated to a steady-state with PKA and ATP. Because this phase of channel activation could take tens of minutes to complete, it was not included in our data presentations. Solution changes were achieved with a fast solution change system (SF-77B; Warner Instruments). The membrane potential was held at −50 mV for all inside-out experiments, and downward deflection indicates CFTR current. All of the currents were recorded with a patch-clamp amplifier (EPC 10; HEKA), filtered with an 8-pole low-pass Bessel filter (Warner Instruments) at 50 Hz, and digitized at 500 Hz using Pulse (V8.80; HEKA) into a PC hard drive.

**Whole-cell mode.** Pipettes used for whole-cell experiments were the same as those used for inside-out exper-

iments except that they were not polished for easier breaking in. The pipette resistance in whole-cell experiments was between 1.5 MΩ and 2.5 MΩ when filled with the whole-cell pipette solution containing (mM) 10 EGTA, 10 HEPES, 20 TEACl, 10 MgATP, 2 $MgCl_2$, 85 aspartate, 16 pyruvate, and 5.8 glucose, with pH adjusted to 7.4 using CsOH. The bath solution was the same as that used in inside-out experiments. After breaking in, the cell at the pipette tip was lifted from the bottom of the chamber to the outlets of the three-barrel glass where the reagents could be immediately perfused to the whole cell. The membrane potential was held at 0 mV throughout the whole recording, and upward deflections represent whole-cell CFTR currents. The whole-cell signals were filtered at 50 Hz and digitized at 2 kHz. All electrophysiological experiments were performed at the room temperature.

### Reagents

PKA, ATP, and cadmium chloride were purchased from Sigma-Aldrich. Cadmium chloride was first prepared as 10 mM stock solution. Upon use, it was diluted into different concentrations using bath or the standard inside-out perfusate subject to mutants under test. CFTR inhibitor-172 (Inh-172) was provided by R. Bridges (Department of Physiology and Biophysics, Rosalind Franklin University, Chicago, IL) with support from Cystic Fibrosis Foundation Therapeutics.

### Data analysis

Figure preparations and curve fittings to generate the time constant, τ, were performed with Igor Pro 6 (WaveMetrics). The cartoon depicting TM1, 6, and 12 in Fig. 1 was prepared with PyMOL (Schrödinger). The second order reaction rates were calculated as $1/(\tau * [Cd^{2+}])$. Student's paired or unpaired *t* tests were performed with Excel (Microsoft), with $P < 0.05$ considered as significant. All data are presented as mean ± SEM. *n* denotes the number of patches for each experiment.

### Online supplemental material

Fig. S1 shows the effects of 5 µM $Cd^{2+}$ on 102C and 341C single mutant currents. Fig. S2 shows the effects of 5 µM $Cd^{2+}$ on 345C and 102C/345C currents. Fig. S3 shows a whole-cell recording of 106C/337C currents in response to forskolin and DTT. Fig. S4 shows reversible inhibition of 107C and 338C single mutant whole-cell currents by 1 mM extracellular $Cd^{2+}$. Fig. S5 presents data suggesting that 341C and 1141C do not coordinate $Cd^{2+}$ together. Fig. S6 shows the effects of 50 µM $Cd^{2+}$ on 1141C current. Fig. S7 shows reversible inhibition of 1144C and 1145C currents by 5 µM $Cd^{2+}$. Fig. S8 shows data suggesting that 95C and 1140C are not close enough to bind one $Cd^{2+}$ ion together. Fig. S9 shows the measurement of the reaction rate between $Cd^{2+}$ and 348C/1141C in the absence of ATP. Online supplemental material is available at http://www.jgp.org/cgi/content/full/jgp.201511557/DC1.

## RESULTS

Although all of our experiments were performed under the cysless background where all 18 endogenous cysteines in CFTR were mutated to serine or leucine (see Materials and methods), as $Cd^{2+}$ can interact with amino acids other than cysteine (Rulíšek and Vondrášek, 1998; Choi et al., 2013), we first tested its effect on the WT cysless CFTR channels. As shown in Fig. 2 A, after phosphorylation-activated WT/cysless CFTR channels were opened by 2 mM ATP in an excised inside-out patch, 5 µM $Cd^{2+}$ applied intracellularly reduced the macroscopic current by 22.8 ± 2.8% ($n = 5$; Fig. 2 C), which was readily reversed upon removal of the metal ion from the solution. Even at a concentration as high as 1 mM, this inhibitory effect of $Cd^{2+}$ vanished within seconds once $Cd^{2+}$ was washed out from the perfusion solution, an observation similar to that in Fig. 2 A except for a slightly higher inhibition of the CFTR current (32.2 ± 9.6%; $n = 5$; Fig. 2, B and C). Although we did not know how and where $Cd^{2+}$ binds to exert this effect, its speedy reversibility within seconds of solution changes indicates a loose binding and allows inferences of the formation of a tight $Cd^{2+}$-binding site by our engineered cysteine pairs, should we observe any $Cd^{2+}$-dependent inhibition that reverses much more slowly. Similar control experiments were performed in whole-cell experiments with WT/cysless channels: in the presence of forskolin, 1 mM $Cd^{2+}$ applied from the extracellular side only induced negligible inhibition of the CFTR current, but the specific CFTR Inh-172 (Ma et al., 2002) abolished nearly all of the current (Fig. 2 D). It is because of such high tolerance of CFTR to external $Cd^{2+}$ that all our following whole-cell experiments adopted this concentration, which helped shorten the recording time so as to maintain a good patch quality.

### Contributions of TM1 and TM6 to the pore's narrow region

As our previous substituted cysteine accessibility method (SCAM) experiments using bulky MTS reagents placed L102 of TM1 and S341 of TM6 at the intracellular edge of the narrow region in the pore (Gao et al., 2013), we first tested whether introducing cysteines at these two positions can craft a tight $Cd^{2+}$-binding site. As a control, the effectiveness of $Cd^{2+}$ on 102C and 341C single mutants was quantified. As shown in Fig. S1, application of 5 µM $Cd^{2+}$ in the continuous presence of ATP decreased 102C and 341C currents by 42.8 ± 2.7% ($n = 5$) and 38.5 ± 3.2% ($n = 3$), respectively. However, subsequent removal of $Cd^{2+}$ in the solution readily recovered the current to the control level in both cases, indicating a relatively weak interaction between $Cd^{2+}$ and either of these two cyst-

eines. In stark contrast, when a double mutant with both 102C and 341C was put to the test, 5 µM $Cd^{2+}$ abolished virtually all of the current (95.6 ± 3%; $n = 3$) in the presence of ATP, and very little current recovered even after tens of seconds of washout with a $Cd^{2+}$-free solution (Fig. 3). We interpreted this result as a tight coordination of one $Cd^{2+}$ ion by the two thiol groups in 102C and 341C, respectively, an idea also supported by the observation of a fast and full recovery of the current by DTT (Fig. 3 A). Because, in order for $Cd^{2+}$ to be coordinated concurrently by two cysteines, the distance between two thiols needs to be <6.5 Å (Jalilehvand et al., 2009), these results place 102C and 341C in close vicinity of each other at the intracellular edge of the narrow region in the pore (see Discussion for more detailed elaborations).

Next we tested whether 102C can form a tight binding site with a cysteine introduced at position 344, a pore-lining residue located one helical turn cytoplasmic to S341 in TM6. Although 5 µM $Cd^{2+}$ only abolished 38.1 ± 5.2% ($n = 6$) of 344C currents, the time course of current recovery upon washout of $Cd^{2+}$ was unusually slow. Specifically, current recovery of other single cysteine mutants upon washout of $Cd^{2+}$ takes place in seconds, whereas it takes tens to hundreds of seconds for 344C currents to recover, suggesting a slow off rate of $Cd^{2+}$ for 344C. However, in light of such a slow off rate, the low inhibition ratio seen with 5 µM $Cd^{2+}$ also indirectly infers a slow apparent on rate of $Cd^{2+}$ for 344C. To better assess the current recovery rate, we increased the concentration of $Cd^{2+}$ to 50 µM, which inhibited 86.4 ± 1.7% ($n = 14$) of 344C currents (Fig. 4 A). Indeed, the current recovery time course after washout of 50 µM $Cd^{2+}$ can be well fitted with a single exponential function yielding a mean time constant of 198 ± 21 s ($n = 8$). Although the reason for the slow on rate and off rate of $Cd^{2+}$ to 344C channels is unclear, 50 µM $Cd^{2+}$ was used for all constructs containing 344C. Interestingly, as seen in Fig. 4 A, DTT was able to expedite the recovery process with a significantly ($P < 0.005$) shorter time constant of 58 ± 11 s ($n = 5$). Because a single cysteine is not expected to afford such a slow off rate for $Cd^{2+}$ (Choi et al., 2013; also see Discussion), these results suggest that 344C may coordinate $Cd^{2+}$ with some endogenous moieties yet to be identified. Nonetheless, if 102C could contribute to this coordination, we would expect an even tighter binding of $Cd^{2+}$ for the double mutant 102C/344C. However, after a nearly full abolition (95.9 ± 1.8%; $n = 7$) of 102C/344C currents by 50 µM $Cd^{2+}$ (Fig. 4 B), upon removal of $Cd^{2+}$, currents recovered with a time constant of 168 ± 24 s ($n = 5$), which is not significantly different from the recovery time constant for the 344C single mutant ($P = 0.57$; Fig. 4 E). In addition, DTT also significantly ($P < 0.001$) shortened the time course of current recovery with an averaged time constant of 43 ± 8 s ($n = 4$; Fig. 4, C and E), which is again not different from that measured with 344C sin-

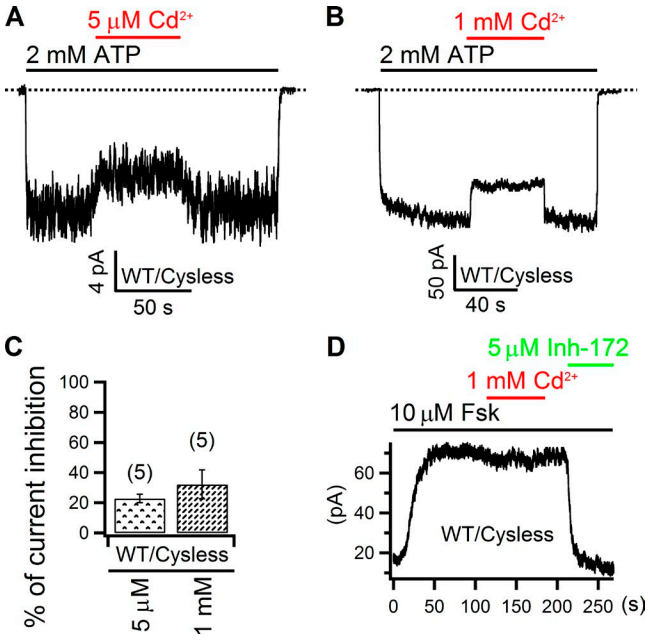


Figure 2. **Effect of $Cd^{2+}$ on WT CFTR channels.** (A and B) Responses of WT cysless channels to 5 µM or 1 mM intracellular $Cd^{2+}$ in inside-out patches. Dashed lines mark the zero current levels (also applicable to all figures). (C) Comparison of effects of intracellular $Cd^{2+}$ on WT cysless CFTR channels. Numbers in parentheses indicate the number of data points (also applicable to all figures). Mean ± SEM is shown. (D) 1 mM $Cd^{2+}$ applied from the extracellular side did not alter whole-cell forskolin-activated CFTR currents.

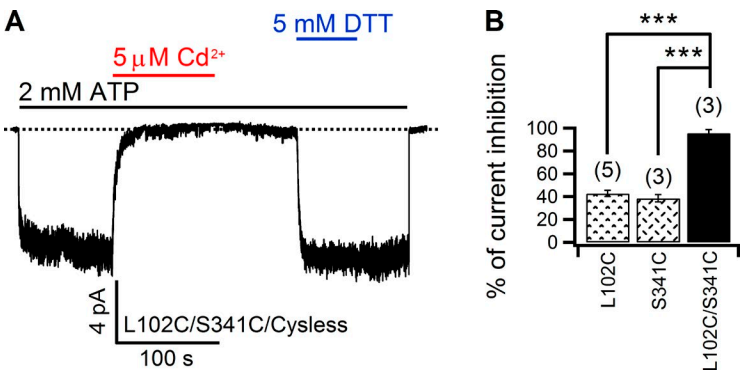


Figure 3. **Cross-linking 102C and 341C with $Cd^{2+}$.** (A) 5 µM $Cd^{2+}$ nearly abolished all 102C/341C currents in an inside-out patch, which recovered at an indiscernible rate upon washout of $Cd^{2+}$ in the presence of EGTA. DTT, however, readily restored the currents. (B) Comparison of $Cd^{2+}$-induced inhibition for 102C, 341C, and 102C/341C. Mean ± SEM is shown. ***, $P < 0.001$.

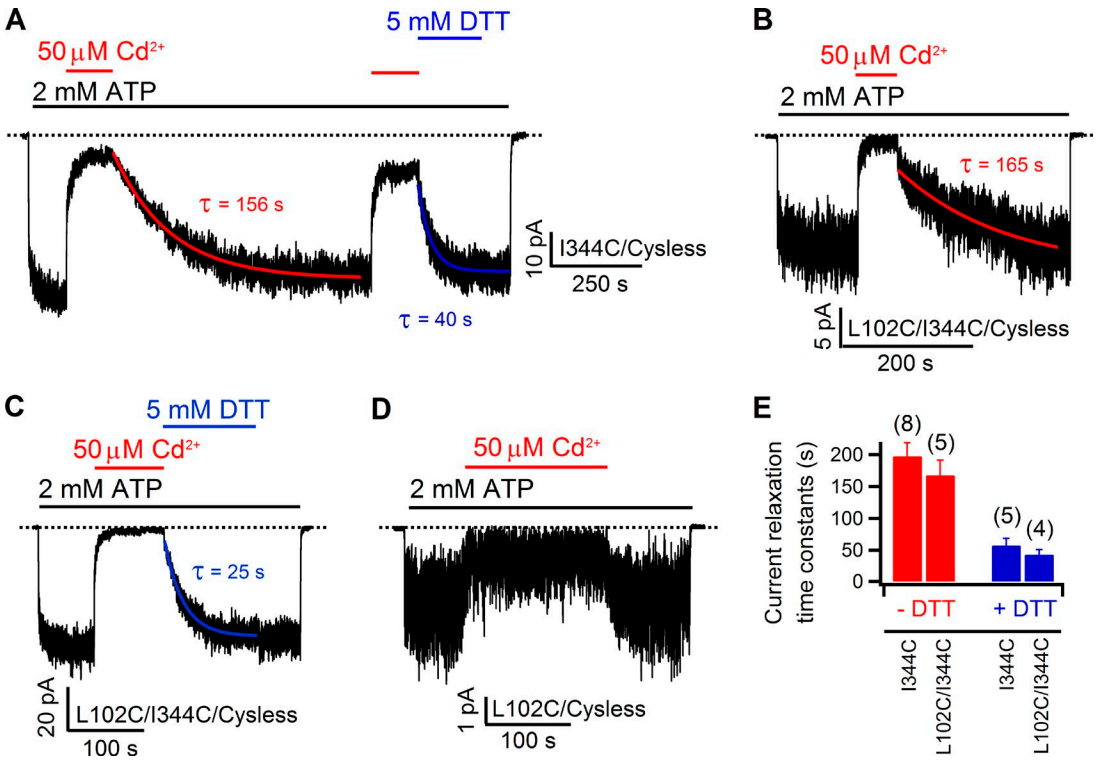


Figure 4. **Effect of $Cd^{2+}$ on double mutant 102C/344C resembles that on 344C single mutant.** (A) Inhibition of 344C currents by $Cd^{2+}$ and slow but discernable recovery from inhibition by $Cd^{2+}$ washout. Note that DTT could speed up the recovery process. Current relaxations were fitted with a single exponential function (red and blue solid curves), yielding the corresponding time constants, τ. (B) Inhibition of 102C/344C currents by 50 μM $Cd^{2+}$. The current relaxation after removal of $Cd^{2+}$ was fitted with a single exponential function (red curve), which yielded a similar time constant as that in the first part in A. (C) Effects of DTT on the current recovery from $Cd^{2+}$-induced inhibition of 102C/344C. In contrast to the recovery phase in the absence of DTT (B), the relaxation time constant generated by the single exponential fitting (blue curve) is much shorter. (D) Effects of 50 μM $Cd^{2+}$ on 102C. (E) Summary of current relaxation time constants for 344C and 102C/344C in the presence or absence of DTT. In both constructs, DTT significantly ($P < 0.005$) decreases τ. Although the relaxation time constants for 102C/344C are slightly smaller than those of 344C, the differences are not statistically significant ($P > 0.1$). Data shown in this figure are from inside-out patches. Mean ± SEM is shown.

gle mutant ($P = 0.36$). Because the inhibition (77.6 ± 5.5%; $n = 4$) on 102C current by 50 μM $Cd^{2+}$ is readily reversible within seconds (Fig. 4 D), the little difference in the effect of $Cd^{2+}$ between 344C and 102C/344C supports the notion that it is 344C with its unknown partner, rather than 102C, that may largely account for the slow recovery seen in 102C/344C double mutants. Thus, despite a confounding effect from a yet to be identified binding partner for $Cd^{2+}$ binding to 344C, these data suggest little contribution of the free energy of binding from 102C to the interaction between $Cd^{2+}$ and the double mutant 102C/344C.

Compared with the complicated interaction between $Cd^{2+}$ and 344C, V345, a neighboring pore-lining residue in TM6, offers another opportunity to address the same issue: whether cysteines placed one helical turn intracellular to S341 are close to 102C in TM1. As shown in Fig. S2, although $Cd^{2+}$-induced inhibition on the double mutant is somewhat higher than that seen with single mutants 102C and 345C (Fig. S2 C), which is perhaps not surprising because the sheer presence of two thiol groups increases the probability of occupancy of the double mutant by $Cd^{2+}$ to disturb the chloride flow in the pore, the fast recovery of the 102C/345C current upon $Cd^{2+}$ washout (Fig. S2 B) led to a tentative conclusion that these two cysteines may not be close enough to coordinate one $Cd^{2+}$ ion (see Discussion for details). Meanwhile, the idea that L102 and S341 are in registry to each other at the intracellular edge of the narrow region is further supported by the findings made on another double mutant, 98C/341C. As shown in Fig. 5, inhibitions by 5 μM $Cd^{2+}$ on 98C (50.4 ± 8.2%; $n = 4$) and 98C/341C (46.4 ± 5.6%; $n = 4$) currents are very similar ($P = 0.7$), and both inhibitions are readily reversed upon removal of the metal ion, indicating that 98C, which is one helical turn cytoplasmic to position 102, is not able to bind a $Cd^{2+}$ ion together with 341C.

Now that two residues at the intracellular edge of the narrow region—position 102 in TM1 and position 341 in TM6—are shown to be aligned closely to each other, under the premise that TM1 and TM6 share a similar secondary structure (Alexander et al., 2009; Bai et al., 2010; El Hiani and Linsdell, 2010; Wang et al., 2011; Gao et al., 2013), residues at the extracellular edge of

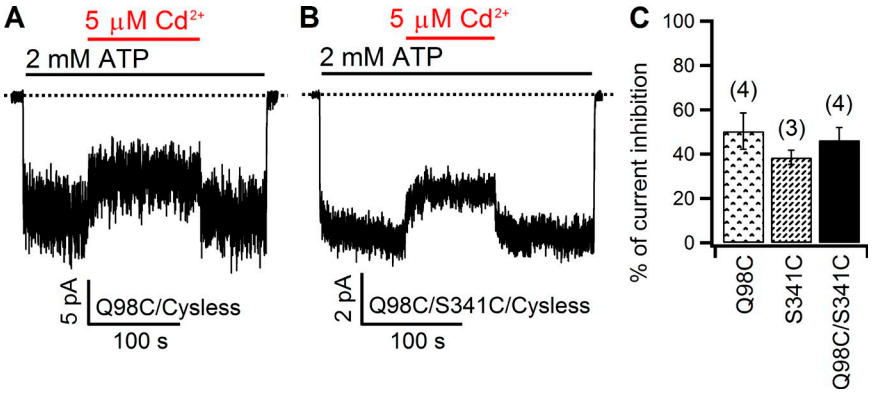


Figure 5. **Comparison of $Cd^{2+}$-induced inhibition between 98C and 98C/341C.** (A and B) In inside-out patches, the inhibitory effect of $Cd^{2+}$ on 98C (A) and 341C (B) currents dissipated in seconds upon removal of $Cd^{2+}$ from the perfusate. (C) Summary of the inhibitory effect of $Cd^{2+}$ on 98C, 341C, and 98C/341C. Note a lack of statistically significant difference in the percent inhibition between the double mutant and either single mutant ($P > 0.3$). Mean ± SEM is shown.

the narrow region in TM1 could also be close to their counterparts in TM6 as the narrowest section in the pore spans only 3–4 amino acids along both TM1 and TM6 (Gao et al., 2013). To test this idea, we introduced cysteines to positions at the extracellular edge of the narrow region in these two segments and assessed their reactivity to $Cd^{2+}$. We set out first with 106C/338C as these two individual positions are extracellularly closest to the narrow region. But unfortunately, this mutant did not yield any measurable current for our whole-cell experiments ($n > 10$), although each single mutant was functional (see below). Therefore, we moved the cysteine in TM6 from position 338 to position 337 to construct a double mutant 106C/337C. As controls, we first tested the effect of extracellular $Cd^{2+}$ on the two single mutants, 106C and 337C. As shown in Fig. 6 A, after whole-cell 106C current was elicited by 10 μM forskolin to a steady-state in the presence of DTT, external application of 1 mM $Cd^{2+}$ nearly abolished all of the 106C current (96.2 ± 0.4%; $n = 4$; Fig. 6 D), which was immediately recovered upon exclusion of $Cd^{2+}$. Subsequent inhibition of the recovered current by Inh-172 (Ma et al., 2002) confirmed that the restored current was indeed from CFTR. As for 337C, $Cd^{2+}$ induced a lower (33.2 ± 2.6%; $n = 7$) but still reversible inhibition (Fig. 6, B and D), and the effect of Inh-172 on this mutant also seemed reduced when compared with that in other whole-cell experiments. These results suggest $Cd^{2+}$ does not bind tightly to either 106C or 337C. However, very interesting experimental results were obtained with the double mutant 106C/337C. First, as shown in Fig. 6 C, in the presence of forskolin, $Cd^{2+}$ applied right after DTT caused an inhibition (90.7 ± 4%; $n = 4$) that was not reversed to an appreciable extent even after washout of the metal ion for tens of seconds, but DTT could readily reverse this inhibition, suggesting that $Cd^{2+}$ is tightly coordinated by 106C and 337C. Second, although forskolin alone could elicit 106C/337C CFTR current, DTT further enhanced this current. Moreover, once DTT was removed, the current started to decay by itself as shown in the red rectangle in Fig. 6 C (also see Fig. S3). One simple explanation for the spontaneous current decay in the absence of the reducing DTT is that these two cysteines form a disulfide bond in a relatively oxidizing extracellular environment, especially in view of the observation that 106C and 337C can be close enough to coordinate a $Cd^{2+}$ ion. Of note, susceptibility of these two cysteines to possible contaminating metals could also diminish the double mutant current (see Liu et al. [2006] for more detailed discussions).

As the A107 residue that neighbors I106 in TM1 also lines the pore, we next tested whether 107C could duplicate what we observed with 106C/337C. When 1 mM $Cd^{2+}$ was applied together with forskolin to cells expressing 107C or 338C, no matter right after forskolin plus DTT or forskolin alone, the whole-cell current was greatly diminished with an averaged inhibition ratio of 93.5 ± 6.6% ($n = 3$) for 107C and 77.1 ± 2.7% ($n = 7$) for 338C (Fig. 7 C and Fig. S4). Because this current inhibition was only seen in the continuous presence of $Cd^{2+}$, we conclude that $Cd^{2+}$ binds loosely to both 107C and 338C. However, the reversal of $Cd^{2+}$-induced inhibition of the double mutant 107C/337C or 107C/338C was only dramatically expedited by DTT (Fig. 7, A and B), indicating a formation of the cysteine–metal–cysteine complex in these two constructs. Therefore, the three testable cysteine pairs—106C/337C, 107C/337C, and 107C/338C—can all craft a tight binding site for $Cd^{2+}$, corroborating the idea that these residues from TM1 and TM6 nestle in a close proximity at the extracellular edge of the narrow region. Together with data on 102C/341C (Fig. 3), we conclude that the narrow region of the pore is flanked internally by L102 and S341 and externally by I106, A107, F337, and T338, a picture consistent with our previous results (Gao et al., 2013; Gao and Hwang, 2015; but cf. Wang et al., 2011).

### Asymmetrical contributions to CFTR's pore by TM6 and TM12

As described in the Introduction, twofold (pseudo) symmetry of the substrate translocation pathway is a hallmark for ABC exporters. For CFTR, all homology models based on ABC exporters' crystal structures also portray a pore so constructed that TM6 and TM12 play

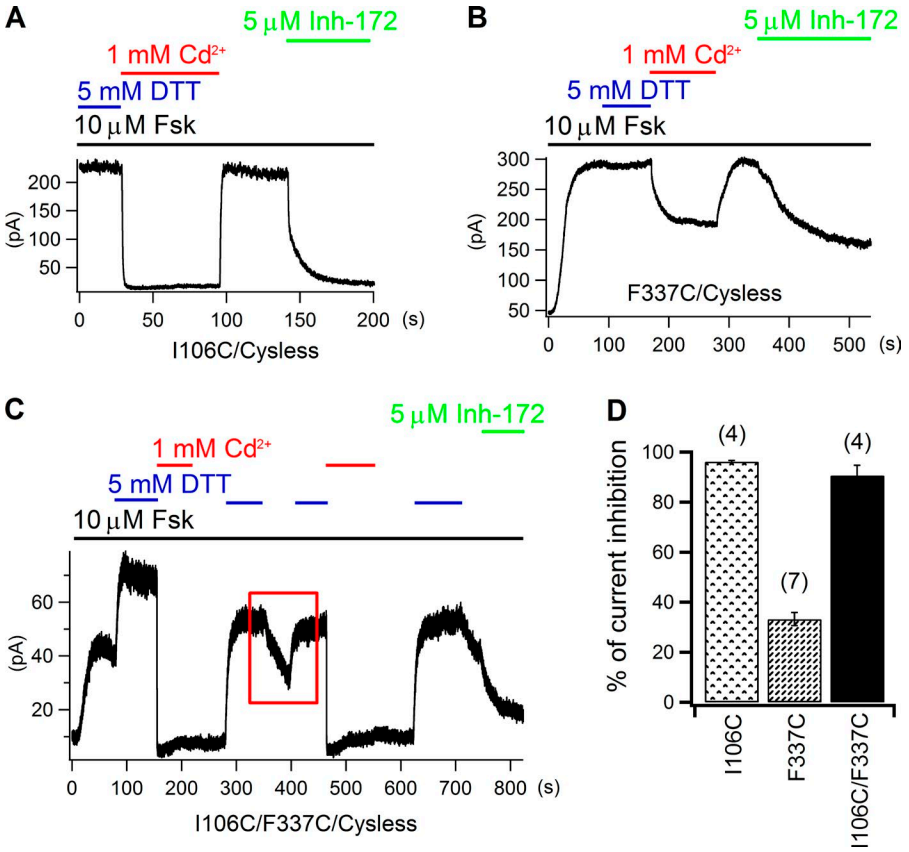


Figure 6. **Cross-linking $Cd^{2+}$ by 106C in TM1 and 337C in TM6.** (A and B) Reversible inhibition of whole-cell 106C (A) and 337C (B) currents by 1 mM of extracellular $Cd^{2+}$. Note that the effect of CFTR inhibitor 172 on 337C is much weaker than that seen with 106C (A). (C) Inhibition of whole-cell 106C/337C current by external $Cd^{2+}$ and DTT-dependent recovery. The red rectangle encloses a part of the recording where current decays by itself when DTT is not present, suggesting possible spontaneous formation of a disulfide bond between 106C and 337C (see Results for details). (D) Averaged current inhibition ratios by external $Cd^{2+}$ for 106C, 337C, and 106C/337C. Mean ± SEM is shown.

a symmetrical structural role (Serohijos et al., 2008; Dalton et al., 2012; Norimatsu et al., 2012; Rahman et al., 2013; Corradi et al., 2015; Mornon et al., 2015). However, such a picture is contested by the following observations. First, unlike that of TM6, the extracellular half of TM12 has been questioned as pore lining (Norimatsu et al., 2012). Second, when carrying out cysteine scanning experiments on TM6 and TM12, Bai et al. (2011) found that cysteines introduced in the topologically defined middle section of TM12 (e.g., 1141C) could be modified by intracellular MTS reagents much faster than those placed in the middle of TM6 (e.g., 341C), suggesting that amino acids in the "middle section" of TM12 may reside in a relatively wider space. We therefore extended our paired cysteine approaches to examine the relative position between TM6 and TM12.

We first tested the cysteine pair 341C/1141C, as previous SCAM data suggest these two positions define the

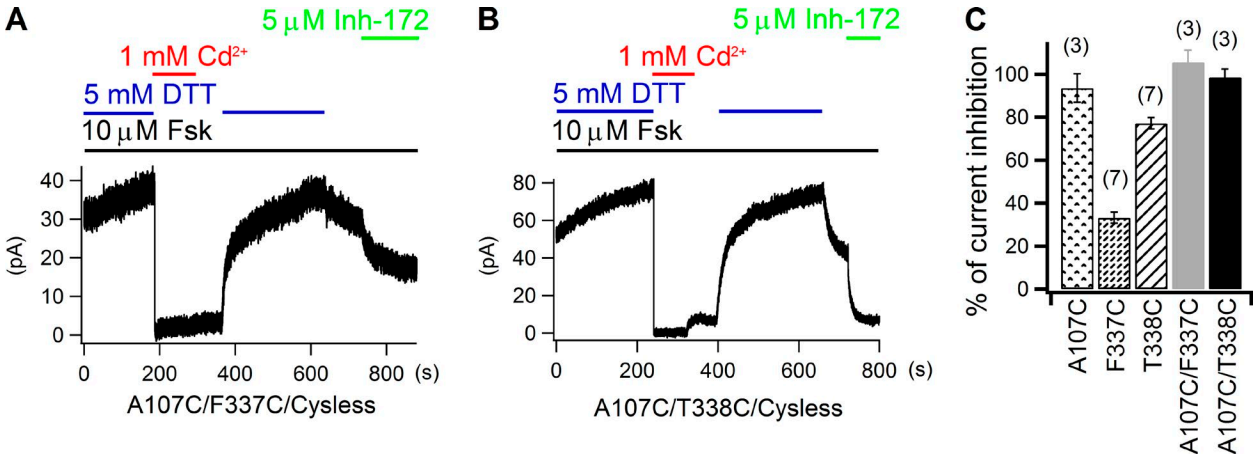


Figure 7. **107C in TM1 can form a multi-liganded $Cd^{2+}$-binding site with either 337C or 338C from TM6.** (A and B) Recovery of $Cd^{2+}$-induced inhibition of 107C/337C (A) and 107C/338C (B) whole-cell currents is dramatically accelerated by DTT. (C) Summary of cadmium's inhibitory effects on 107C, 337C, 338C, 107C/337C, and 107C/338C currents. Mean ± SEM is shown.

internal access limits in TM6 and TM12, respectively (Alexander et al., 2009; Bai et al., 2010, 2011). However, inhibition of the double mutant 341C/1141C (54.9 ± 4.5%; $n$ = 4) by internal application of 5 µM $Cd^{2+}$ was only slightly larger than those on single mutants 341C (38.5 ± 3.2%; $n$ = 3) or 1141C (44.4 ± 3.5%; $n$ = 5; Fig. S5). More importantly, washout of $Cd^{2+}$ resulted in an immediate recovery of the current for either single or double mutant. Next, we moved the cysteine in TM6 to positions one helical turn cytoplasmic to construct two double mutants—344C/1141C and 345C/1141C. For 344C/1141C, although, upon application of 50 µM $Cd^{2+}$, the current was almost fully inhibited (99.1 ± 0.3%; $n$ = 5); simple washing out of $Cd^{2+}$ with ATP recovered the double mutant current with a mean time constant of 219 ± 23 s ($n$ = 6). Meanwhile, DTT could greatly speed up this process with a time constant of 42 ± 7 s ($n$ = 5; Fig. 8 A). These time constants are not statistically different from those of 344C single mutant (Fig. 4 E). In view of the ready recovery of 1141C current after removal of 50 µM $Cd^{2+}$ (Fig. S6), we again proposed that 344C and its "invisible partner" could account for the slow recovery of 344C/1141C current. As for 345C/1141C, 5 µM $Cd^{2+}$ evoked an inhibition (48.4 ± 7.1%; $n$ = 4) that is not much different from that of 1141C (Fig. S5 C). More importantly, the immediate recovery of the double mutant current upon exclusion of $Cd^{2+}$ from the solution prompted us to conclude that 345C and 1141C are not able to provide a bi-dentate $Cd^{2+}$-binding site (Fig. 8 C).

These results suggest that position 1141 in the middle of TM12 does not align with position 341, 344, or 345 of TM6. In contrast, the data shown in Fig. 9 lead to the conclusion that position 1141 is in registry with position 348, which is two helical turns cytoplasmic to position 341 in TM6. Specifically, the recovery rate of the $Cd^{2+}$-inhibited current upon simple removal of $Cd^{2+}$ was too slow to be measureable; however, DTT greatly accelerated the current recovery (Fig. 9 B). In addition, 5 µM $Cd^{2+}$ caused an inhibition of 88.6 ± 2.7% ($n$ = 5) of the 348C/1141C current, which is much higher than that seen with either corresponding single mutant (Fig. 9 C). Although the aforementioned data put M348 in the close vicinity of S1141, a position close to the middle of TM12, examination of 348C/1144C and 348C/1145C with $Cd^{2+}$ provided further insights into the relative alignment between TM6 and TM12. As shown in Fig. S7, both 1144C and 1145C currents could be readily inhibited by 5 µM $Cd^{2+}$, but a fast relief of the inhibition was also seen upon washout of $Cd^{2+}$ in both cases. However, this is not the case for 348C/1144C (Fig. 10 A). Besides a higher inhibition ratio of the mean current induced by $Cd^{2+}$ (Fig. 10 D), the recovery from the inhibited state takes a long time (hundreds of seconds) to reach its steady-state. Fitting the recovery time course with a

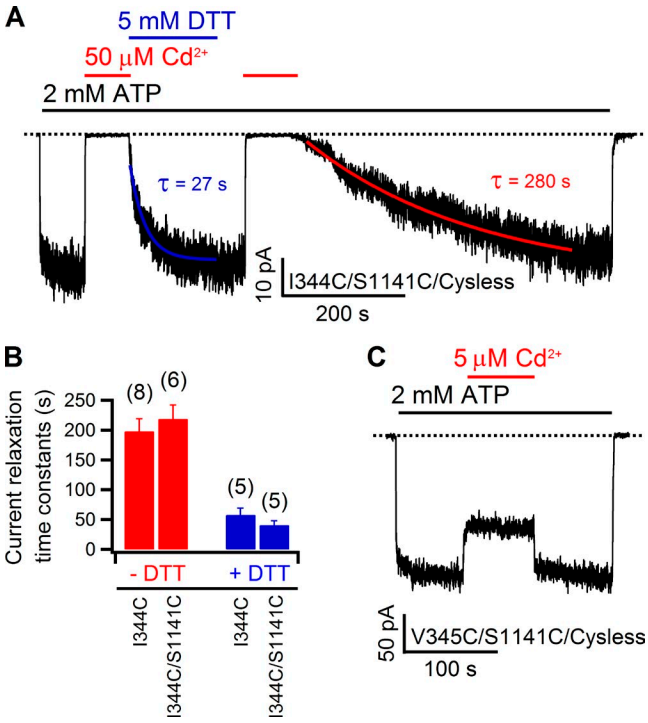


Figure 8. **Effect of 50 µM $Cd^{2+}$ on 344C/1141C and 345C/1141C.** (A) In an inside-out patch, 50 µM $Cd^{2+}$ inhibited 344C/1141C currents almost to the baseline, but removal of the metal ion results in a slow current relaxation that can be accelerated by DTT. The time constants were obtained by fitting corresponding current relaxation curves with single exponential functions. (B) The current relaxation time constants on 344C/1141C and 344C are similar (P = 0.51 for without DTT and P = 0.26 for with DTT, respectively), indicating introduction of 1141C does not increase the binding affinity of $Cd^{2+}$ to 344C. Thus, position 344 may not be close to position 1141. Mean ± SEM is shown. (C) In an inside-out recording, 5 µM $Cd^{2+}$ induced reversible inhibition on 345C/1141C, suggesting 345C and 1141C are not able to construct a bi-dentate $Cd^{2+}$-binding site.

single exponential function yielded a time constant of 182 ± 30 s ($n$ = 5), which is significantly shortened by DTT (40 ± 7 s; $n$ = 4; Fig. 10, A and B), suggesting that 348C and 1144C can coordinate a single $Cd^{2+}$ ion, but the 348C–$Cd^{2+}$–1144C complex is not as strong as the 348C–$Cd^{2+}$–1141C metal bridge (Fig. 9). In contrast, results with 348C/1145C double mutant were similar to those of 348C/1141C (Fig. 10 C). Collectively, these data suggest that the topologically defined middle segment of TM12 is not aligned with that of TM6 (i.e., position 341), but rather with a position that is two helical turns cytoplasmic to position 341 (i.e., position 348). More interestingly, such an alignment between TM6 and TM12 is further supported by the observations made on another double mutant formed by 95C (TM1) and 1141C. Specifically, although $Cd^{2+}$-induced inhibition on 95C (34.6 ± 4.2%; $n$ = 7) could be readily released within seconds upon washing $Cd^{2+}$ out with a solution with

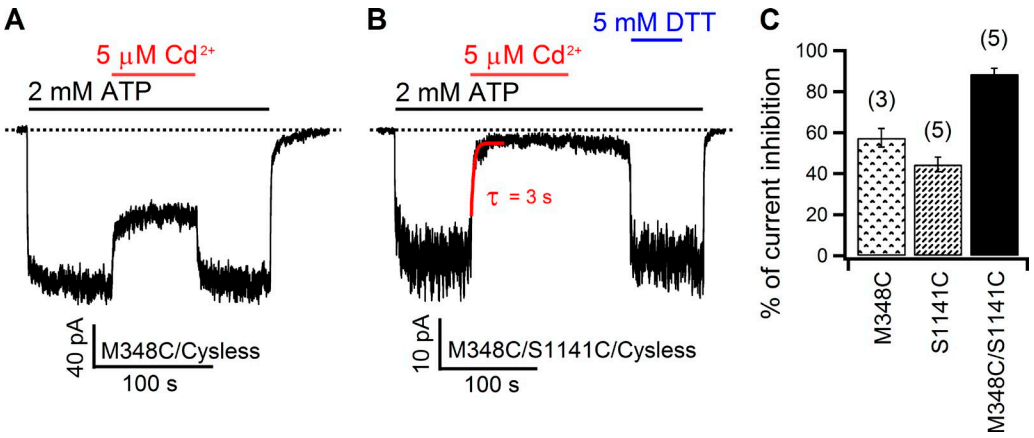


Figure 9. **348C, but not 341C, of TM6 can tightly coordinate $Cd^{2+}$ with 1141C of TM12.** (A) An inside-out recording shows that the inhibition of 341C/1141C currents was subject to the continuous presence of $Cd^{2+}$ in the solution. (B) Contrary to that shown in A, for the double mutant 348C/1141C, the current inhibition brought by $Cd^{2+}$ in an inside-out patch was reversed extremely slowly by simple washout, but DTT rapidly restored the current. The current decay phase was fitted with a single exponential function (see Fig. S9 for more details). (C) Summary of the percent inhibition of 348C, 1141C, and 348C/1141C currents by 5 μM $Cd^{2+}$. Mean ± SEM is shown.

EGTA (Fig. 11 A), reversal of the much higher inhibition (92.9 ± 2.1%; $n$ = 7) seen with the 95C/1141C double mutant took a much longer time, as indicated by the current recovery time constants (84 ± 15 s; $n$ = 8). However, such a time course could be greatly shortened by the metal chelator DTT (6 ± 1 s; $n$ = 5; Fig. 11, B and C), suggesting the formation of a $Cd^{2+}$ bridge between 95C and 1141C. Thus, position 1141 in TM12 registers with both position 95 in TM1 and position 348 in TM6; they are all located two helical turns cytoplasmic to the internal edge of the narrow region. Collectively, these data support a picture that the nominal counterparts—TM6 and TM12—do not contribute to CFTR's pore symmetrically.

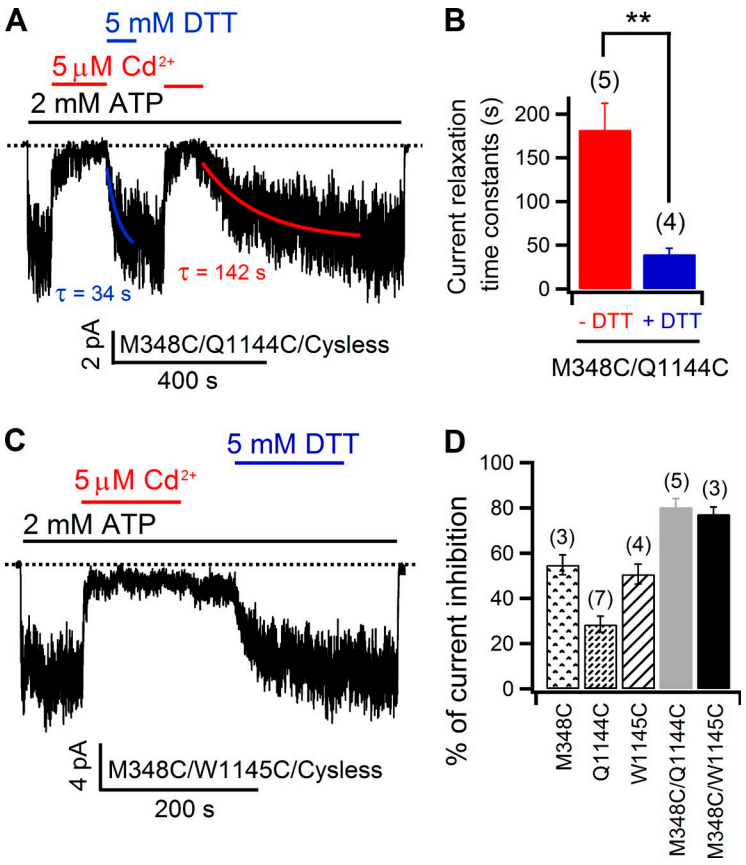


Figure 10. **348C of TM6 forms a tight $Cd^{2+}$-binding site with either 1144C or 1145C of TM12.** (A) Acceleration of current recovery from $Cd^{2+}$-induced inhibition of 348C/1144C currents by DTT in an inside-out recording. Although 348C/1144C currents could recover from the $Cd^{2+}$-inhibited state irrespective of the presence of DTT, comparison of the time constants generated by fitting both current relaxations with a single exponential function (red and blue solid curves) indicates DTT can accelerate such a process. (B) Comparison of 348C/1144C current relaxation time constants indicates there is significant difference when DTT is in the solution. **, $P < 0.01$. (C) DTT-dependent recovery of 348C/1145C inside-out current after $Cd^{2+}$ application implicates a tight $Cd^{2+}$-binding site constructed by these two cysteines. (D) Summary of effect of $Cd^{2+}$ on each mutant as indicated in the panel. Mean ± SEM is shown.

## DISCUSSION

Site-directed mutagenesis offers investigators a unique tool to study the spots of interest in an ion channel protein by allowing them to replace original amino acids with others and examine post hoc the functional consequences of these mutation-induced perturbations with single-molecule patch-clamp techniques. SCAM has supplemented this already powerful combination as the result of a rapid reaction of cysteine's thiol group with swaths of thiol-specific modification reagents (Wilson and Karlin, 1998; Serrano et al., 2006). In the past two decades, this method has been implemented successfully in the studies of structure/function of CFTR. Especially because of the known molecular sizes of these bulky reagents, one can also, to some extent, use them to gauge the physical dimension of the pore. Consequently, a rough picture of an hourglass-shaped pore for CFTR has subsequently emerged (see Introduction). In contrast, reducing the size of the probe to approximate that of a permeating anion (e.g., $[Au(CN)_2]^-$) can afford "chemical scanning" along the whole ion permeation pathway (Serrano et al., 2006). Such an effective application of the permeant thiol-specific reagents enabled our latest localization of a gate in CFTR (Gao and Hwang, 2015).

Moreover, by engineering cysteine pairs, one cannot only take advantage of the potential for disulfide bond formation between two thiol groups in a close proximity, but also use a broad array of soft metals (e.g., $Cd^{2+}$) as a tool to cross-link two cysteines that may not be close enough to form a disulfide bond. Indeed, a series of elegant studies by Yellen's group on potassium channels and hyperpolarization-activated cation (HCN) channels showed that $Cd^{2+}$ could be tightly coordinated by multiple physically close cysteines or histidines to irreversibly alter the channel's gating or permeation properties (Yellen et al., 1994; Liu et al., 1997; Holmgren et al., 1998; del Camino and Yellen, 2001; Rothberg et al., 2002, 2003; Webster et al., 2004; Ryu and Yellen, 2012). Similar strategies of engineering cysteine pairs have also been adopted by several groups in the CFTR field with fruitful results. For example, by engineering cysteine pairs in the head, central, and tail regions of CFTR's two NBDs, Mense et al. (2006) demonstrated that the two NBDs in CFTR can form a head to tail "heterodimeric" complex upon ATP binding, which likely resembles those observed in other ABC proteins. Guided by a homology model built using the crystal structure of Sav 1866 as the template, Riordan's group introduced cysteine pairs into the cytoplasmic–membrane domain interface and successfully identified several potential contact sites between NBDs and TMDs (He et al., 2008; Serohijos et al., 2008). In addition, a recent study, by engineering cysteine pairs in the extracellular loop, provided evidence for electrostatic interactions at the outer mouth of the pore (Cui et al., 2014).

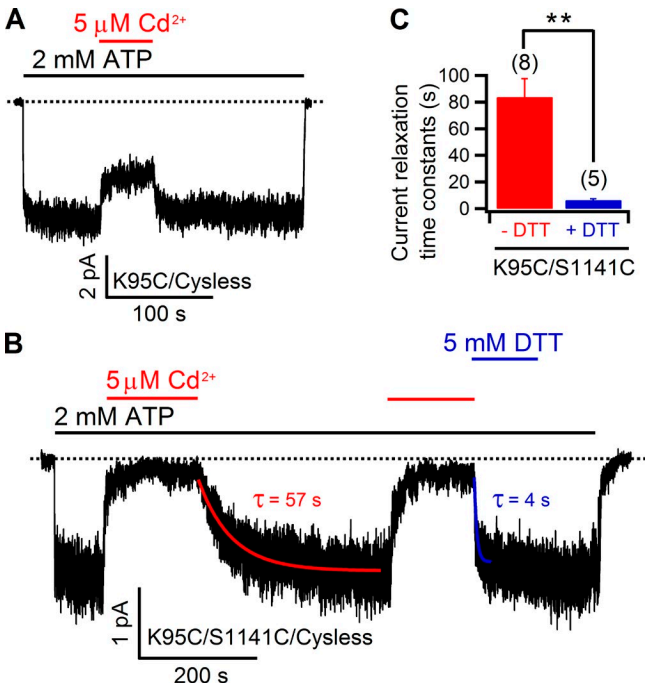


Figure 11. **Positive contribution of 95C in TM1 to $Cd^{2+}$ binding to 1141C in TM12.** (A) Reversible inhibition of 95C inside-out currents by $Cd^{2+}$. (B) After $Cd^{2+}$-induced inhibition, 95C/1141C currents can recover at a discernable rate back to the preinhibition level by simple $Cd^{2+}$ removal; in the same inside-out patch, current recovery is dramatically accelerated by DTT. Time constants were generated from fitting both current relaxations with a single exponential function (red and blue curves). (C) Summary of the relaxation time constants for current recovery in the presence or absence of DTT. Mean ± SEM is shown. **, $P < 0.01$. Here, we need to point out that, although another study drew the same conclusion that position 95 is close to position 1141 in the pore (El Hiani and Linsdell, 2014), observations made between the current study and that study are somewhat different. Specifically, in El Hiani and Linsdell (2014), both 95C and 95C/1141C currents were increased upon $Cd^{2+}$ exposure, opposite to what we observed. The reason behind this discrepancy is unclear, but numerous differences in SCAM results have been noted before in the literature (Bai et al., 2010, 2011; El Hiani and Linsdell, 2010; Qian et al., 2011; Wang et al., 2011; Gao et al., 2013). Regardless, because the interaction between $Cd^{2+}$ and the binding site constructed by 95C and 1141C is relatively weak judged from a relatively faster relaxation time constant, when compared with other positive pairs in the current study (e.g., 102C/341C), we wondered whether moving the cysteine at position 1141 to its neighboring positions (i.e., 1140C or 1142C) could potentially identify a tighter binding site for $Cd^{2+}$ with the 95C background. Unfortunately, although the 95C/1142C double mutant failed to yield any current in our experiments ($n > 10$), 95C/1140C seems less likely to compose such a tight binding site we sought (see Fig. S8).

However, we were surprised that very few studies actually implement this strategy to tackle CFTR's TMDs, especially because a low sequence similarity between CFTR's TMDs and those of other ABC proteins should

pose a tremendous challenge to rely solely on computational approaches to gain a molecular understanding of the structure/function relation for CFTR's TMDs. We therefore adopted the paired cysteine method to investigate TM–TM interactions with a focus on the three most extensively studied pore-lining TMs in our laboratory—TM1, 6, and 12 (Bai et al., 2010, 2011; Gao et al., 2013). Of note, a recent study has provided evidence for positive interactions among these three TMs (El Hiani and Linsdell, 2014). Although their primarily interested candidates are residues lining the inner vestibule of CFTR's pore, we made a deliberate decision to place an emphasis on residues around the narrow region for the following reason. It is generally accepted that the inner and outer vestibules in CFTR's pore are spacious, but the narrow region in between should bear a width that is <5.3 Å based on the permeability ratio measured among different anions (Linsdell et al., 1997), making $Cd^{2+}$ an ideal cross-linker at the two edges of this restrictive region.

To our delight, 102C in TM1 and 341C in TM6 indeed form a tight binding site for $Cd^{2+}$ applied from the intracellular side of the membrane (Fig. 3). The inferred physical proximity between these two positions not only corroborates our previous conclusion (Gao et al., 2013) that L102, originally assigned to define the external end of CFTR's TM1 based on hydropathy analysis (Riordan et al., 1989), should instead be placed at the internal edge of the narrow region similar to S341 in TM6 (Bai et al., 2010), but also demonstrates that both TM1 and TM6 contribute to the internal end of the narrow region. Moreover, the observation that cysteine pairs (including 106C/337C, 107C/337C, and 107C/338C) introduced three to five residues external to L102 and S341, respectively, can tightly coordinate $Cd^{2+}$ applied from the extracellular side of the membrane supports the notion that residues from TM1 and TM6 also flank the external edge of the narrow region (Alexander et al., 2009; Bai et al., 2010; Gao et al., 2013). Thus, given that both TM1 and TM6 also harbor additional residues that build the internal and external vestibules, we posit that both TM1 and TM6 span the whole length of CFTR's anion permeation pathway (also see Gao and Hwang [2015]).

However, the almost irreversible binding of $Cd^{2+}$ with the aforementioned cysteine pairs is puzzling as such tight binding of a $Cd^{2+}$ ion is reserved for a preferred tetrahedral coordination seen in numerous metalloproteins (Rulíšek and Vondrášek, 1998). Indeed, the formation of a $Cd^{2+}$-binding site of covalent bond strength with four cysteines has been shown in several ion channel studies (Yellen et al., 1994; Webster et al., 2004). Noticeably, a recent study by Choi et al. (2013) reported an off rate constant ($k_{off}$) of $3.5 \times 10^{-2}$ $s^{-1}$ for two cysteines that are cross-linkable in the staphylococcal α-hemolysin (αHL) transmembrane pore, which corresponds to a dissociation time constant of ∼29 s. Thus, although the pore structure of CFTR is different from that of αHL, it is likely that the positive pairs we identified (e.g., 102C/341C) borrow some additional help from some yet to be identified elements in the pore so that they can together construct a binding site that has a much higher affinity for $Cd^{2+}$ than one constructed by two lone cysteines. Moreover, the idea that other chemical moieties in CFTR's pore may participate in coordinating $Cd^{2+}$ may also explain the observation that recovery of the single cysteine mutant 344C currents from $Cd^{2+}$-induced inhibition takes hundreds of seconds to complete (Fig. 4 A), which is in stark contrast to that shown in Choi et al. (2013) (a time constant of <0.08 s for single cysteine in αHL). Notwithstanding, introduction of an additional cysteine—102C—did not seem to alter coordination of $Cd^{2+}$ by 344C and its yet to be identified partners, suggesting that, unlike positions 102 and 341, 102C and 344C may not be close enough to coordinate one $Cd^{2+}$ ion. Interestingly, if we accept the premises that the diameter of the narrow region is ∼5.3 Å, as indicated above, and that both TM1 and TM6 assume the same α-helical structure with a pitch of 5.4 Å, then the diagonal distance (>7.5 Å assuming a vertical triangle formed by residues 102, 341, and 344) between 102C and 344C should exceed that required for a multi-liganded $Cd^{2+}$-binding site (Fig. 4). The same geometric predictions can be made for cysteine pairs 102C/345C and 98C/341C. Indeed, our data (Fig. 5 and Fig. S2) show no evidence for a cooperative binding of $Cd^{2+}$ by any of these two paired cysteines. In contrast, we found experimental evidence for a close proximity among four positions at the external end of the narrow region along TM1 and TM6 (i.e., 106C/337C, 107C/337C, and 107C/338C). Thus, the very region defining the narrowest section of the pore is made partly by TM1 and TM6 over a distance of one helical pitch or 5.4 Å.

Although the well-known coordination chemistry of $Cd^{2+}$ with the cysteine thiols affords a more exquisite structural interpretation for a relatively compact environment where the space between each party is constrained, this favorable attribute of physical constraint is lost once we move our discussion focus to a more spacious compartment of CFTR's pore—the inner vestibule. Nonetheless, we were surprised by the extremely slow off rates of $Cd^{2+}$ in several of the engineered cysteine pairs (e.g., 348C/1141C and 348C/1145C), suggesting the presence of binding partners other than the introduced thiols in the inner vestibule. Although more extensive future studies on the mechanism of this apparent tight $Cd^{2+}$ binding are needed, the current data do reveal an unexpected role played by TM12 in the pore. Specifically, our data in Fig. 9 place 1141C of TM12 in close vicinity to 348C, contradicting the proposition that position 1141 in TM12, like its counterpart S341 in

TM6, may be close to the internal brink of the narrow region (Bai et al., 2010, 2011). Then, results in Fig. 10 further suggest 348C may straddle between 1141C and 1144C (or 1145C), which may line on the same face of two adjacent helical turns. This geometrical constrain subsequently predicts that S1141 should be located one to two helical turns away from the narrow region of the pore. Interestingly, 1141C indeed contributes to $Cd^{2+}$ binding to 95C (Fig. 11), a position two helical turns internal to L102 of TM1 that defines the internal edge of the narrow region. Collectively, these data lead to a surprising picture for the structural role of CFTR's TM12: the middle section of TM12 (i.e., S1141) is located two helical turns cytoplasmically from the proposed inner brim of the narrow segment of the pore.

Before we wrap up our discussion, a few subjects should be revisited and/or inspected in a more critical manner so that the readers are fully aware of the potential caveats in our approach. First, although the marker used in the current study to judge the formation of a tight $Cd^{2+}$-binding site is the sluggishness of current recovery after washout of $Cd^{2+}$, a fast recovery from the $Cd^{2+}$-inhibited state for several double mutant currents (e.g., 102C/345C) may not necessarily indicate a physical alienation between the two cysteines involved, especially when a higher inhibition for double mutant was observed, as in the case of 102C/345C. One possible scenario is that even though the two cysteines in the double mutant are close to each other, a lack of support from the aforementioned unidentified partner(s) could render the $Cd^{2+}$-binding site as weak as undetectable in our experiments.

Second, we need to point out that our measurements of $Cd^{2+}$-induced current reductions (summarized in Table 1 for the positive pairs) and current recovery afterward with or without DTT do not tell whether the effect of $Cd^{2+}$ is on gating or ion conduction, or both. Because all of the residues examined in the current study have been shown to line the pore, we prefer a simple pore-plugging effect. Of note, this distinction becomes murkier when dealing with positions close to the narrow region of the pore because of a possible dual function for this segment (Gao and Hwang, 2015). However, even if the effect of $Cd^{2+}$ in some of our mutants is attributed to gating perturbation, the identification of positive pairs still attests to a physical proximity for the introduced cysteine pair during certain states of the gating cycle. On the other hand, because $Cd^{2+}$ was always applied in the presence of ATP for an extended period of time during which the channel can virtually visit all possible gating states, negative results obtained in our experiments suggest that the two residues under study are not close at any given point in a gating cycle, thus excluding certain structural configurations for the channel. Moreover, as many of our double mutant constructs exhibit extremely slow apparent off rates of $Cd^{2+}$, we need to be concerned by the possibility that this strong force may actually allow the formation of the inferred metal bridge in conformations in fact rarely visited during normal gating transitions. Nevertheless, this worse scenario is probably avoided as most of the inhibition occurred within seconds of $Cd^{2+}$ applications and the gating cycle of CFTR is $\sim 1\ s^{-1}$.

Table 1. **Summary of current inhibition by $Cd^{2+}$ on mutants carrying cross-linkable cysteine pairs**

| Cysteine pairs | % Inhibition |
|---|---|
| **TM1/TM6** | |
| 102C/341C | 95.6 ± 3 |
| 106C/337C | 90.7 ± 4 |
| 107C/337C | 105.6 ± 5.5 |
| 107C/338C | 98.6 ± 3.8 |
| **TM6/TM12** | |
| 348C/1141C | 88.6 ± 2.7 |
| 348C/1144C | 80.3 ± 3.7 |
| 348C/1145C | 77.2 ± 3.1 |
| **TM1/TM12** | |
| 95C/1141C | 92.9 ± 2.1 |

Note that the >100% inhibition with 107C/337C results from the observations in some experiments where the current level in the presence of $Cd^{2+}$ is even lower than that at the beginning of the recording or under CFTR Inh-172.

Third, except for the 348C/1141C pair, most of the double mutants were not able to generate large enough currents in inside-out patches for us to test state-dependent effects of $Cd^{2+}$. However, we do realize that the state-dependent data could shed more light as channel gating is a dynamic process. Therefore, whenever possible, we also directed our efforts to provide our audience with a sliver of this kind of structural insights. For example, the second order rate constant for $Cd^{2+}$ reactivity with 348C/1141C mutant in the absence of ATP is approximately threefold higher than that with ATP (Fig. 9 and Fig. S9), suggesting these two cysteines may be either in a more accessible location or better orientated to coordinate $Cd^{2+}$ in the closed state. Besides, we also observed, in our whole-cell recordings of 106C/337C channels, a biphasic current response to forskolin application: current increase followed by a decrease, which could suggest that these two cysteines are close to each other only in the open state of CFTR (see Fig. S3 legend for more details).

Bearing nearly all of the topological hallmarks of an ABC exporter, CFTR is a bona fide member of this superfamily, as previous phylogenetic study has suggested (Dean and Annilo, 2005). Many functional data on CFTR's NBDs and TMDs also support the hypothesis that CFTR evolved from an ABC exporter by degenerating its intracellular gate (Bai et al., 2011). We noticed that, because of CFTR's kinship with ABC transporters, nearly all homology models of CFTR were built using the crystal structures of ABC exporters as templates (Serohijos et al., 2008; Dalton et al., 2012; Norimatsu et al., 2012; Rahman et al., 2013; Mornon et al., 2015). Unsur-

prisingly, although many models are able to account for those identified pore-lining components in individual TMs, few could achieve a satisfaction from all examining eyes, partly because of their confinement to the two-fold pseudo-symmetry inherited in ABC transporters (e.g., the one in Fig. 1). Therefore, by providing some physical constraints between well-defined, paired positions in different TMs, data reported here could provide an effective guide for future computational modeling.

## ACKNOWLEDGMENTS

This work was supported by the National Institutes of Health (NIH; grant NIHR01DK55835) and the Cystic Fibrosis Foundation (grant Hwang11P0) to T.-C. Hwang. This investigation was conducted in a facility constructed with support from the National Center for Research Resources (NIH) Research Facilities Improvement Program (grant C06 RR-01648901).

During the course of this study, 5% of T.-C. Hwang's salary was supported by Vertex Pharmaceutical Inc. The authors declare no additional competing financial interests.

Merritt Maduke served as editor.

Submitted: 10 December 2015
Accepted: 28 March 2016

## REFERENCES

Akabas, M.H., C. Kaufmann, T.A. Cook, and P. Archdeacon. 1994. Amino acid residues lining the chloride channel of the cystic fibrosis transmembrane conductance regulator. *J. Biol. Chem.* 269:14865–14868.

Alexander, C., A. Ivetac, X. Liu, Y. Norimatsu, J.R. Serrano, A. Landstrom, M. Sansom, and D.C. Dawson. 2009. Cystic fibrosis transmembrane conductance regulator: using differential reactivity toward channel-permeant and channel-impermeant thiol-reactive probes to test a molecular model for the pore. *Biochemistry.* 48:10078–10088. http://dx.doi.org/10.1021/bi901314c

Aller, S.G., J. Yu, A. Ward, Y. Weng, S. Chittaboina, R. Zhuo, P.M. Harrell, Y.T. Trinh, Q. Zhang, I.L. Urbatsch, and G. Chang. 2009. Structure of P-glycoprotein reveals a molecular basis for poly-specific drug binding. *Science.* 323:1718–1722. http://dx.doi.org/10.1126/science.1168750

Bai, Y., M. Li, and T.C. Hwang. 2010. Dual roles of the sixth transmembrane segment of the CFTR chloride channel in gating and permeation. *J. Gen. Physiol.* 136:293–309. http://dx.doi.org/10.1085/jgp.201010480

Bai, Y., M. Li, and T.C. Hwang. 2011. Structural basis for the channel function of a degraded ABC transporter, CFTR (ABCC7). *J. Gen. Physiol.* 138:495–507. http://dx.doi.org/10.1085/jgp.201110705

Chen, T.Y., and T.C. Hwang. 2008. CLC-0 and CFTR: chloride channels evolved from transporters. *Physiol. Rev.* 88:351–387. http://dx.doi.org/10.1152/physrev.00058.2006

Choi, L.S., T. Mach, and H. Bayley. 2013. Rates and stoichiometries of metal ion probes of cysteine residues within ion channels. *Biophys. J.* 105:356–364. http://dx.doi.org/10.1016/j.bpj.2013.04.046

Choudhury, H.G., Z. Tong, I. Mathavan, Y. Li, S. Iwata, S. Zirah, S. Rebuffat, H.W. van Veen, and K. Beis. 2014. Structure of an antibacterial peptide ATP-binding cassette transporter in a novel outward occluded state. *Proc. Natl. Acad. Sci. USA.* 111:9145–9150. http://dx.doi.org/10.1073/pnas.1320506111

Cooper, E.C., and L.Y. Jan. 1999. Ion channel genes and human neurological disease: recent progress, prospects, and challenges. *Proc. Natl. Acad. Sci. USA.* 96:4759–4766. http://dx.doi.org/10.1073/pnas.96.9.4759

Corradi, V., P. Vergani, and D.P. Tieleman. 2015. Cystic fibrosis transmembrane conductance regulator (CFTR): closed and open state channel models. *J. Biol. Chem.* 290:22891–22906. http://dx.doi.org/10.1074/jbc.M115.665125

Csanády, L., and D.C. Gadsby. 1999. CFTR channel gating: Incremental progress in irreversible steps. *J. Gen. Physiol.* 114:49–54. http://dx.doi.org/10.1085/jgp.114.1.49

Cui, G., K.S. Rahman, D.T. Infield, C. Kuang, C.Z. Prince, and N.A. McCarty. 2014. Three charged amino acids in extracellular loop 1 are involved in maintaining the outer pore architecture of CFTR. *J. Gen. Physiol.* 144:159–179. http://dx.doi.org/10.1085/jgp.201311122

Dalton, J., O. Kalid, M. Schushan, N. Ben-Tal, and J. Villà-Freixa. 2012. New model of cystic fibrosis transmembrane conductance regulator proposes active channel-like conformation. *J. Chem. Inf. Model.* 52:1842–1853. http://dx.doi.org/10.1021/ci2005884

Dawson, R.J., and K.P. Locher. 2006. Structure of a bacterial multidrug ABC transporter. *Nature.* 443:180–185. http://dx.doi.org/10.1038/nature05155

Dean, M., and T. Annilo. 2005. Evolution of the ATP-binding cassette (ABC) transporter superfamily in vertebrates. *Annu. Rev. Genomics Hum. Genet.* 6:123–142. http://dx.doi.org/10.1146/annurev.genom.6.080604.162122

del Camino, D., and G. Yellen. 2001. Tight steric closure at the intracellular activation gate of a voltage-gated $K^+$ channel. *Neuron.* 32:649–656. http://dx.doi.org/10.1016/S0896-6273(01)00487-1

El Hiani, Y., and P. Linsdell. 2010. Changes in accessibility of cytoplasmic substances to the pore associated with activation of the cystic fibrosis transmembrane conductance regulator chloride channel. *J. Biol. Chem.* 285:32126–32140. http://dx.doi.org/10.1074/jbc.M110.113332

El Hiani, Y., and P. Linsdell. 2014. Metal bridges illuminate transmembrane domain movements during gating of the cystic fibrosis transmembrane conductance regulator chloride channel. *J. Biol. Chem.* 289:28149–28159. http://dx.doi.org/10.1074/jbc.M114.593103

Gadsby, D.C., and A.C. Nairn. 1999a. Control of CFTR channel gating by phosphorylation and nucleotide hydrolysis. *Physiol. Rev.* 79:S77–S107.

Gadsby, D.C., and A.C. Nairn. 1999b. Regulation of CFTR Cl− ion channels by phosphorylation and dephosphorylation. *Adv. Second Messenger Phosphoprotein Res.* 33:79–106. http://dx.doi.org/10.1016/S1040-7952(99)80006-8

Gadsby, D.C., P. Vergani, and L. Csanády. 2006. The ABC protein turned chloride channel whose failure causes cystic fibrosis. *Nature.* 440:477–483. http://dx.doi.org/10.1038/nature04712

Gao, X., and T.C. Hwang. 2015. Localizing a gate in CFTR. *Proc. Natl. Acad. Sci. USA.* 112:2461–2466. http://dx.doi.org/10.1073/pnas.1420676112

Gao, X., Y. Bai, and T.C. Hwang. 2013. Cysteine scanning of CFTR's first transmembrane segment reveals its plausible roles in gating and permeation. *Biophys. J.* 104:786–797. http://dx.doi.org/10.1016/j.bpj.2012.12.048

He, L., A.A. Aleksandrov, A.W. Serohijos, T. Hegedus, L.A. Aleksandrov, L. Cui, N.V. Dokholyan, and J.R. Riordan. 2008. Multiple membrane-cytoplasmic domain contacts in the cystic fibrosis transmembrane conductance regulator (CFTR) mediate regulation of channel gating. *J. Biol. Chem.* 283:26383–26390. http://dx.doi.org/10.1074/jbc.M803894200

Hohl, M., C. Briand, M.G. Grütter, and M.A. Seeger. 2012. Crystal structure of a heterodimeric ABC transporter in its inward-facing conformation. *Nat. Struct. Mol. Biol.* 19:395–402. http://dx.doi.org/10.1038/nsmb.2267

Holmgren, M., K.S. Shin, and G. Yellen. 1998. The activation gate of a voltage-gated $K^+$ channel can be trapped in the open state by an intersubunit metal bridge. *Neuron.* 21:617–621. http://dx.doi.org/10.1016/S0896-6273(00)80571-1

Jalilehvand, F., B.O. Leung, and V. Mah. 2009. Cadmium(II) complex formation with cysteine and penicillamine. *Inorg. Chem.* 48:5758–5771. http://dx.doi.org/10.1021/ic802278r

Jih, K.Y., and T.C. Hwang. 2012. Nonequilibrium gating of CFTR on an equilibrium theme. *Physiology (Bethesda).* 27:351–361. http://dx.doi.org/10.1152/physiol.00026.2012

Jin, M.S., M.L. Oldham, Q. Zhang, and J. Chen. 2012. Crystal structure of the multidrug transporter P-glycoprotein from *Caenorhabditis elegans*. *Nature.* 490:566–569. http://dx.doi.org/10.1038/nature11448

Kodan, A., T. Yamaguchi, T. Nakatsu, K. Sakiyama, C.J. Hipolito, A. Fujioka, R. Hirokane, K. Ikeguchi, B. Watanabe, J. Hiratake, et al. 2014. Structural basis for gating mechanisms of a eukaryotic P-glycoprotein homolog. *Proc. Natl. Acad. Sci. USA.* 111:4049–4054. http://dx.doi.org/10.1073/pnas.1321562111

Krężel, A., W. Lesniak, M. Jezowska-Bojczuk, P. Mlynarz, J. Brasuñ, H. Kozlowski, and W. Bal. 2001. Coordination of heavy metals by dithiothreitol, a commonly used thiol group protectant. *J. Inorg. Biochem.* 84:77–88. http://dx.doi.org/10.1016/S0162-0134(00)00212-9

Linsdell, P. 2014. Functional architecture of the CFTR chloride channel. *Mol. Membr. Biol.* 31:1–16. http://dx.doi.org/10.3109/09687688.2013.868055

Linsdell, P., J.A. Tabcharani, J.M. Rommens, Y.X. Hou, X.B. Chang, L.C. Tsui, J.R. Riordan, and J.W. Hanrahan. 1997. Permeability of wild-type and mutant cystic fibrosis transmembrane conductance regulator chloride channels to polyatomic anions. *J. Gen. Physiol.* 110:355–364. http://dx.doi.org/10.1085/jgp.110.4.355

Liu, X., S.S. Smith, and D.C. Dawson. 2003. CFTR: what's it like inside the pore? *J. Exp. Zoolog. A Comp. Exp. Biol.* 300A:69–75. http://dx.doi.org/10.1002/jez.a.10311

Liu, X., C. Alexander, J. Serrano, E. Borg, and D.C. Dawson. 2006. Variable reactivity of an engineered cysteine at position 338 in cystic fibrosis transmembrane conductance regulator reflects different chemical states of the thiol. *J. Biol. Chem.* 281:8275–8285. http://dx.doi.org/10.1074/jbc.M512458200

Liu, Y., M. Holmgren, M.E. Jurman, and G. Yellen. 1997. Gated access to the pore of a voltage-dependent $K^+$ channel. *Neuron.* 19:175–184. http://dx.doi.org/10.1016/S0896-6273(00)80357-8

Ma, T., J.R. Thiagarajah, H. Yang, N.D. Sonawane, C. Folli, L.J. Galietta, and A.S. Verkman. 2002. Thiazolidinone CFTR inhibitor identified by high-throughput screening blocks cholera toxin-induced intestinal fluid secretion. *J. Clin. Invest.* 110:1651–1658. http://dx.doi.org/10.1172/JCI0216112

Mense, M., P. Vergani, D.M. White, G. Altberg, A.C. Nairn, and D.C. Gadsby. 2006. In vivo phosphorylation of CFTR promotes formation of a nucleotide-binding domain heterodimer. *EMBO J.* 25:4728–4739. http://dx.doi.org/10.1038/sj.emboj.7601373

Mornon, J.P., B. Hoffmann, S. Jonic, P. Lehn, and I. Callebaut. 2015. Full-open and closed CFTR channels, with lateral tunnels from the cytoplasm and an alternative position of the F508 region, as revealed by molecular dynamics. *Cell. Mol. Life Sci.* 72:1377–1403. http://dx.doi.org/10.1007/s00018-014-1749-2

Norimatsu, Y., A. Ivetac, C. Alexander, J. Kirkham, N. O'Donnell, D.C. Dawson, and M.S. Sansom. 2012. Cystic fibrosis transmembrane conductance regulator: a molecular model defines the architecture of the anion conduction path and locates a "bottleneck" in the pore. *Biochemistry.* 51:2199–2212. http://dx.doi.org/10.1021/bi201888a

Qian, F., Y. El Hiani, and P. Linsdell. 2011. Functional arrangement of the 12th transmembrane region in the CFTR chloride channel pore based on functional investigation of a cysteine-less CFTR variant. *Pflugers Arch.* 462:559–571. http://dx.doi.org/10.1007/s00424-011-0998-2

Rahman, K.S., G. Cui, S.C. Harvey, and N.A. McCarty. 2013. Modeling the conformational changes underlying channel opening in CFTR. *PLoS One.* 8:e74574. http://dx.doi.org/10.1371/journal.pone.0074574

Riordan, J.R., J.M. Rommens, B. Kerem, N. Alon, R. Rozmahel, Z. Grzelczak, J. Zielenski, S. Lok, N. Plavsic, J.L. Chou, et al. 1989. Identification of the cystic fibrosis gene: cloning and characterization of complementary DNA. *Science.* 245:1066–1073. http://dx.doi.org/10.1126/science.2475911

Rothberg, B.S., K.S. Shin, P.S. Phale, and G. Yellen. 2002. Voltage-controlled gating at the intracellular entrance to a hyperpolarization-activated cation channel. *J. Gen. Physiol.* 119:83–91. http://dx.doi.org/10.1085/jgp.119.1.83

Rothberg, B.S., K.S. Shin, and G. Yellen. 2003. Movements near the gate of a hyperpolarization-activated cation channel. *J. Gen. Physiol.* 122:501–510. http://dx.doi.org/10.1085/jgp.200308928

Rulíšek, L., and J. Vondrášek. 1998. Coordination geometries of selected transition metal ions ($Co^{2+}$, $Ni^{2+}$, $Cu^{2+}$, $Zn^{2+}$, $Cd^{2+}$, and $Hg^{2+}$) in metalloproteins. *J. Inorg. Biochem.* 71:115–127. http://dx.doi.org/10.1016/S0162-0134(98)10042-9

Ryu, S., and G. Yellen. 2012. Charge movement in gating-locked HCN channels reveals weak coupling of voltage sensors and gate. *J. Gen. Physiol.* 140:469–479. http://dx.doi.org/10.1085/jgp.201210850

Serohijos, A.W., T. Hegedus, A.A. Aleksandrov, L. He, L. Cui, N.V. Dokholyan, and J.R. Riordan. 2008. Phenylalanine-508 mediates a cytoplasmic-membrane domain contact in the CFTR 3D structure crucial to assembly and channel function. *Proc. Natl. Acad. Sci. USA.* 105:3256–3261. http://dx.doi.org/10.1073/pnas.0800254105

Serrano, J.R., X. Liu, E.R. Borg, C.S. Alexander, C.F. Shaw III, and D.C. Dawson. 2006. CFTR: Ligand exchange between a permeant anion ($[Au(CN)2]^-$) and an engineered cysteine (T338C) blocks the pore. *Biophys. J.* 91:1737–1748. http://dx.doi.org/10.1529/biophysj.105.078899

Sheppard, D.N., and K.A. Robinson. 1997. Mechanism of glibenclamide inhibition of cystic fibrosis transmembrane conductance regulator $Cl^-$ channels expressed in a murine cell line. *J. Physiol.* 503:333–346. http://dx.doi.org/10.1111/j.1469-7793.1997.333bh.x

Shintre, C.A., A.C. Pike, Q. Li, J.I. Kim, A.J. Barr, S. Goubin, L. Shrestha, J. Yang, G. Berridge, J. Ross, et al. 2013. Structures of ABCB10, a human ATP-binding cassette transporter in apo- and nucleotide-bound states. *Proc. Natl. Acad. Sci. USA.* 110:9710–9715. http://dx.doi.org/10.1073/pnas.1217042110

Wang, W., Y. El Hiani, and P. Linsdell. 2011. Alignment of transmembrane regions in the cystic fibrosis transmembrane conductance regulator chloride channel pore. *J. Gen. Physiol.* 138:165–178. http://dx.doi.org/10.1085/jgp.201110605

Wang, W., Y. El Hiani, H.N. Rubaiy, and P. Linsdell. 2014. Relative contribution of different transmembrane segments to the CFTR chloride channel pore. *Pflugers Arch.* 466:477–490. http://dx.doi.org/10.1007/s00424-013-1317-x

Wang, Y., T.W. Loo, M.C. Bartlett, and D.M. Clarke. 2007. Correctors promote maturation of cystic fibrosis transmembrane conductance regulator (CFTR)-processing mutants by binding to the protein. *J. Biol. Chem.* 282:33247–33251. http://dx.doi.org/10.1074/jbc.C700175200

Ward, A., C.L. Reyes, J. Yu, C.B. Roth, and G. Chang. 2007. Flexibility in the ABC transporter MsbA: Alternating access with a twist. *Proc. Natl. Acad. Sci. USA.* 104:19005–19010. http://dx.doi.org/10.1073/pnas.0709388104

Webster, S.M., D. Del Camino, J.P. Dekker, and G. Yellen. 2004. Intracellular gate opening in Shaker $K^+$ channels defined by high-affinity metal bridges. *Nature*. 428:864–868. http://dx.doi.org/10.1038/nature02468

Wilson, G.G., and A. Karlin. 1998. The location of the gate in the acetylcholine receptor channel. *Neuron*. 20:1269–1281. http://dx.doi.org/10.1016/S0896-6273(00)80506-1

Yellen, G., D. Sodickson, T.Y. Chen, and M.E. Jurman. 1994. An engineered cysteine in the external mouth of a K+ channel allows inactivation to be modulated by metal binding. *Biophys. J.* 66:1068–1075. http://dx.doi.org/10.1016/S0006-3495(94)80888-4

Zhang, J., and T.C. Hwang. 2015. The fifth transmembrane segment of cystic fibrosis transmembrane conductance regulator contributes to its anion permeation pathway. *Biochemistry*. 54:3839–3850. http://dx.doi.org/10.1021/acs.biochem.5b00427

Zhou, Z., S. Hu, and T.C. Hwang. 2002. Probing an open CFTR pore with organic anion blockers. *J. Gen. Physiol.* 120:647–662. http://dx.doi.org/10.1085/jgp.20028685